MasterChem: Cooking 2D-Polymers

D. Rodríguez-San-Miguel,[a,b] P. Amo-Ochoa[a] and F. Zamora[a,b,*]

2D-polymers are still dominated by graphene and closely related materials such as boron nitride, transition metal sulphides and oxides. However, the rational combination of molecules with suitable design is already showing the high potential of chemistry in this new research field. The aim of this feature article is to illustrate, and provide some perspectives, the current state-of-the-art in the field of synthetic 2D-polymers showing different alternatives to prepare this novel type of polymers based on the rational use of chemistry. This review comprises a brief revision of the essential concepts, the strategies of preparation following the two general approaches, bottom-up and top-down, and a revision of the promising seminal properties showed by some of these nanomaterials.

1. Introduction

A 2D-polymer can be easily defined as a combination of repeat units in two spatial directions to generate a monolayer of atomic or molecular thickness.[1] The layer formation is based on a suitable combination of planar molecules or entities (for example: metal fragments) on a topological plane. There are some clear criteria that a 2D-polymer has to fulfil such as: *i*) planarity in the sense of topologically planar sheets, *ii*) structural order or crystallinity of its repeat units, *iii*) mono-atomic or -molecular thickness, and *iv*) free-standing integrity which is related with its strength. As a result a 2D-polymer should present considerably larger dimensions in the plane, named as lateral dimensions, *versus* its thickness. Schlüter *et al*. have recently published an excellent review describing structural and topological aspects concerning 2D-polymers which is complementary to our feature article.[2]

Still the most paradigmatic case of a 2D-polymer is the case of graphene.[3] Indeed the isolation of graphene and the characterization of its unique physical properties has motivated an unprecedented research activity in this field. A natural extension for the search of alternative materials to graphene has been focused on purely inorganic materials. Over 40 single-layer materials coming from this family of materials have been isolated and characterized, being among others boron nitride, MoS_2, and black phosphorous a representation of the most studied due to their promising physical properties and potential applications.[4, 5] However the lack of structural chemical design of these polymers has suggested the use of synthetic materials in order to face/overcome this drawback.

In parallel to the increasing scientific and even technological interest of these purely inorganic materials, very recently a major breakthrough has showed the high potential of organic synthesis to produce the first samples of synthetic 2D-polymers showing how chemistry can play a major role in this new scenario of material science. In this context a simple and suitable approach to produce 2D-polymers arises from the basic concept based on the connection of selected molecules, with suitable symmetry, and by means of reversible bonds that can allow self-reparation and, therefore, the formation of well-ordered structures. These are the basic ideas behind the relatively new and important type of mesoporous materials: Coordination Polymers (CPs) focus on Metal-Organic Frameworks (MOFs) and Covalent Organic Frameworks (COFs). MOFs and COFs share some common features since both are mesoporous materials based on cross-linked polymers with long-range periodicity based on the connection of their building-blocks. The key factor determining their crystallinity is based on the use of reversible bonds. An excellent review discussing bonding aspects in detail has recently been published by Colson and Dichtel.[6] However, the differences are relative to the constituents, MOFs use metal fragments and organic ligands as building blocks, while COFs are based on the combination of organic molecules. Therefore, despite some similarities as soft-designed porous materials, COFs show much higher thermal and chemical stability. But in terms of structural capabilities both MOFs and COFs are able to produce a large structural variety using conventional and well-established criteria of coordination and organic synthesis.

As we describe in the following sections there is still not a single example neither of a MOF nor of a COF that fulfils the requirements to be considered a 2D-polymer. However, there are several examples showing the production of ordered

[a] *Departamento de Química Inorgánica and Condensed Matter Physics Center (IFIMAC). Universidad Autónoma de Madrid (UAM), 28049 Madrid, Spain. E-mail: felix.zamora@uam.es*

[b] *Instituto Madrileño de Estudios Avanzados en Nanociencia (IMDEA Nanociencia). 28049 Madrid, Spain.*

laminar structures with a thickness corresponding to few layers. This is indeed another aspect of high interest from materials science point of view, the production of materials containing a limited number of 2D-polymers, but still with structural order, crystallinity. The idea of control over thickness for the production of a variety of 2D-few layers materials is not new, since it was highlighted by R. Feynman "What could we do with layered structures with just the right layers? What would the properties of materials be if we could really arrange the atoms the way we want them? They would be very interesting to investigate theoretically. I can't see exactly what would happen, but I can hardly doubt that when we have some control of the arrangement of things on a small scale we will get an enormously greater range of possible properties that substances can have, and of different things that we can do"[7] and a clear example showing the high interest in terms of physical properties is graphene: single vs double, triple, few graphene layers.

Finally, we have to make clear a concept that will appear along this manuscript and that we have named as "monolayer 2D-material", to be consistent with the review of Schlüter *et al.*, related with single layers of materials whose structures are still not perfectly established. In general, the problems concerning structural characterization can be intrinsic to the single layer, named structural defects, or related to the use of a suitable experimental technique able to provide this information.

In summary, the aim of this feature article is to provide a tool to envision a spread of the current limited number of available 2D-polymers. We describe the current state-of-the-art of what chemistry is bringing to this new multidisciplinary field of nano- and materials science, summarizing the preparation methods and the characterization techniques that have been already used.

2. Preparation Methods

2.1 Bottom-up

The bottom-up methodologies are very appealing because in most of the cases they are technically simple and, therefore, powerful tools towards potential applications. Additionally, under the suitable experimental conditions, the materials that can be generated by these approaches, can get into very large lateral dimensions. They are essentially based on the direct combination/reaction of different building blocks allowing the formation of two-dimensional structures in both MOFs and COFs. Typically, this can be either carried out on a surface, with a certain assistance of the surface in the process, or at the liquid-liquid or liquid-air interface.

2.1.1 Metal-Organic Frameworks

On-surface synthesis. On-surface synthesis of MOFs is a well-stablished field. To the best of our knowledge, preparation of single layers has been limited to ultrahigh vacuum conditions and subsequent scanning tunnelling microscope (STM) characterization. The architectures of the layers formed under these specific conditions are very broad going from hexagonal, square, rectangular, etc., with an excellent control of the design of the cavity in shape and chemical functionalization as well as in size. However, the final results of the materials show very limited lateral dimensions. Additionally the so-formed single-layers have never been transferred out of the ultrahigh vacuum chamber therefore limiting their physical characterization and potential device fabrication. Consequently we will not consider this method as a tool for the production of 2D-polymers based on MOFs.

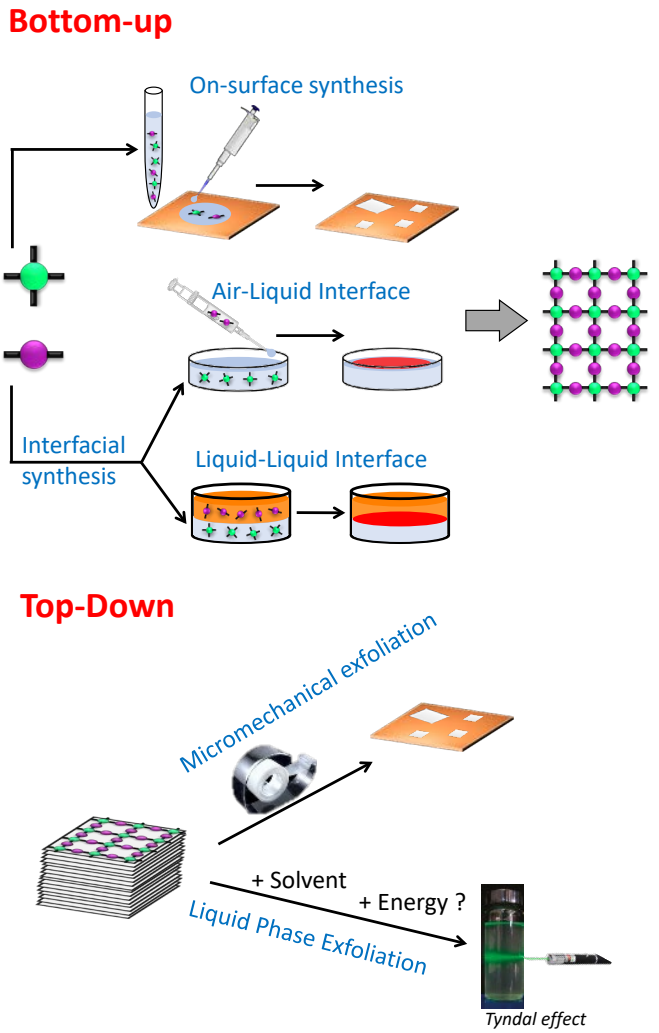

Fig. 1 Scheme of the strategies already developed to produce single or few layers of MOFs and COFs.

Synthesis at water/air or solvent-to-solvent interface. Langmuir–Blodgett (LB) method at the water/air interface. In an unprecedented work *Schlüter et al*. published the synthesis of a monolayer of a dense coordination polymer (CP) at the water/air interface.[8] The method was based on the reaction between a hexafunctional terpyridine (tpy)-based organic precursor dissolved in chloroform and dropwise deposited on top of a water solution containing a Fe^{2+} salt. Fast solvent evaporation of the chloroform produces the confinement of the

organic ligand in two dimensions, over the water layer due to the very low solubility of the *tpy*, prior to polymerization. The ligand was compressed up to 10 mNm^{-1} and the polymerization spread at the air-water interface on a Langmuir–Blodgett trough. As a result, formation of a homogeneous monolayer of the dense coordination polymer $[Fe^{II}_2(tpy)^{4+}]_n$, (0<x<3), is formed and vertically transferred to several substrates. Atomic force microscopy (AFM) confirms isolation of partially folded sheets monolayer while deposition of the monolayer on a transmission electron microscopy (TEM) grid demonstrates that it is mechanically stable to span over 20×20 μm^2 holes (Fig. 2). Optical microscopy and TEM images show coverage of areas > 500×500 μm^2. Similar results were obtained with other metal salts such as Ru^{2+} or Zn^{2+}. However, in this work they do not provide structural evidences of the 2D polymer integrity.

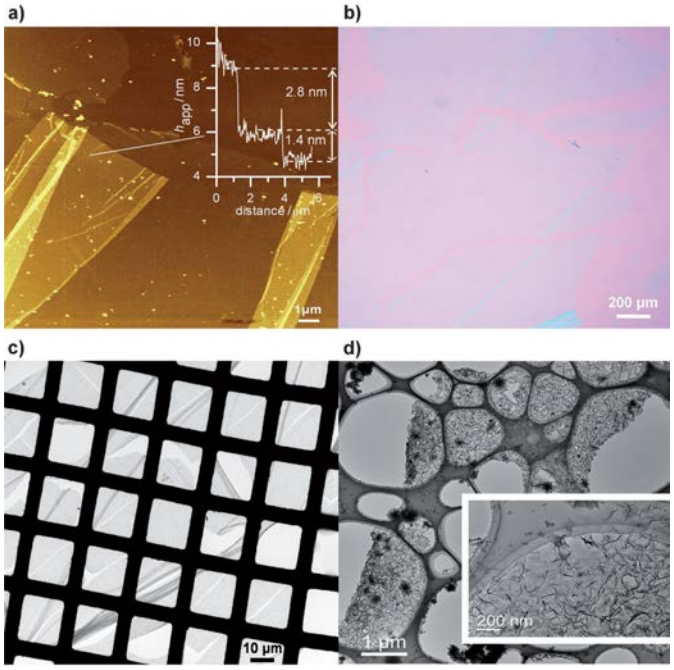

Fig. 2 Microscopy images of the dense coordination polymer $[Fe^{II}(tpy)^{4+}]_n$ (0<x<3) sheet. a) AFM image and its height profile (inset) and b) optical image after transfer to SiO_2. c) TEM image after horizontal transfer from top onto a Cu grid with holes. d) TEM images at two different magnifications. Figure taken from Ref. 8 with permission.

This work was further extended showing the reaction of a oligofunctional terpyridine-based ligands spread at an air-water interface, with transition metal salts, such as Fe(II), Co(II/III), Zn(II), and Pb(II), dissolved in the water.[9] After the water surface was pressured to 10 mNm^{-1}, formation of layers of a series of CPs takes place. AFM characterization of the sheets transferred to SiO_2 confirms formation of monolayers which are mechanically stable to be transferred to TEM grids with 20×20 μm^2 holes. Interestingly, AFM indentation experiments allow to estimate the in-plane elastic modulus, which is coherent with other sheets such as graphene. Additionally, the CP sheets were also useful to build up multilayer assemblies on square centimetre length scales on solid substrates using layer-by-layer deposition method.

Following the same fabrication procedure the hexafunctional terpyridine (tpy) monolayer with Zn(II), $[Zn_2(tpy)^{4+}]_n$, was transferred into a centimetre sized quartz substrate (Fig. 3). The immersion of this substrate into a Fe(II) water solution produces a Fe(II) monolayer *via* trasmetalation.[10] Ultraviolet (UV) and raman spectra confirm the transformation while X-ray photoelectron spectroscopy (XPS) allows to quantify the Zn(II) to Fe(II) metal substitution in *ca*. 60 %. Additionally, predetermined patterns defined by photolithography were used to create monolayer sheets composed of different net-points. This novel patterned net-points can be considered as two-dimensional analogues of linear copolymers.

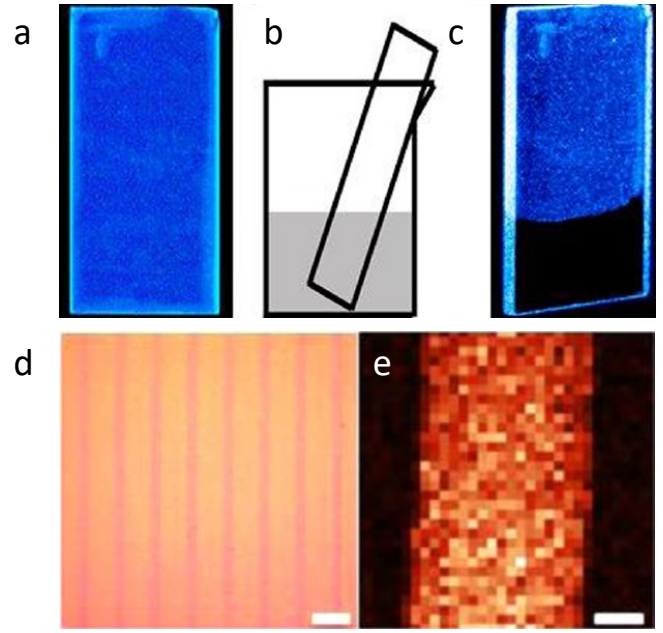

Fig. 3 (a) Fluorescent monolayer sheet of $[Zn_2(tpy)^{4+}]_n$ on quartz (*ca*. 4 cm^2), (b) scheme of the dipping procedure to affect transmetalation, and (c) the sheet after 1 h partial exposure to a 0.1 mol L^{-1} $(NH_4)_2Fe(SO_4)_2$ solution in water. Optical (d) and Raman microscopy (e) images of $[Zn_2(tpy)^{4+}]_n$ on SiO_2/Si substrate. Figure adapted from Ref. 10 with permission.

In terms of potential applications this result represents a significant advance in monolayer and polymer chemistry with applications in fields such as surface coating, molecular electronics, device fabrication, imaging and sensing. Despite of the breakthrough that these works represented, the main inconvenient was the concerns relative to the internal order of the monolayers due to the lack of experimental data (eg. X-ray diffraction, STM, …).

Nishihara *et al*. have reported the formation of a nickel bis(dithiolene) single-layer sheet using a similar procedure, water/air interface, but with the advantage that the single layer was formed under atmospheric pressure instead of the pressure required using Langmuir-Blodgett (Fig. 4a).[11] AFM images confirm the monomolecular thickness of the π-conjugated sheet and lateral dimensions over tens of square microns (Fig. 4b,c). Importantly, STM images show the expected hexagonal arrangement and some degree of structural order (Fig. 4d). As a result of the high electron delocalization in the structure of this sheet, reversible redox behaviour was expected. Indeed, cyclovoltammetry carried out on the sheets deposited on highly oriented pyrolytic graphite (HOPG)

confirms that the oxidation state of the sheets can be reversible modulated, redox switching.

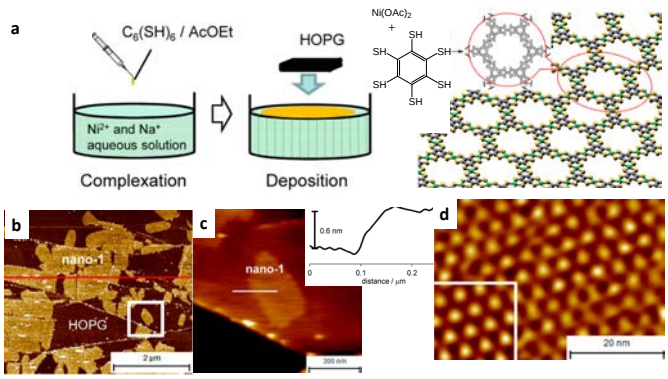

Fig. 4 a) Scheme of the single layer fabrication process and the structure of the nickel bis(dithiolene) layer. b,c) Phase and topological AFM images showing sheets on HOPG, and a characteristic height profile of a single layer. d) STM image of sheets on HOPG showing a hexagonal pattern. Adapted with permission of Ref. 11 with permission.

Very recently Feng *et al*. have used the same procedure to form a single-layer sheet consisting of nickel bis(dithiolene) complexes at the air-water interface.[12] The ligand used in this case was the 1,2,5,6,9,10-triphenylenehexathiol (THT) which shows a large π-conjugated structure (Fig. 5). The confirmation of single layer formation and isolation was done by a combination of optical microscopy, SEM and AFM images (Fig. 5 b-d). XPS was successfully used to confirm the chemical composition of the monolayers as well as an unique coordination environment for Ni(II). Interestingly, the multilayer structures with controllable numbers of layers could be readily deposited on substrates by a repeated LB transfer process. Additionally the transfer process on Cu grids shows free-standing single layers confirming their mechanical stability. Importantly, electron diffraction shows the typical hexagonal diffraction pattern expected for this structure with hexagonal order (Fig. 5a).

In a recent work, the direct reaction between a complex three-way dipyrrin ligand (**L1**) and zinc(II) acetate carried out at the air-water interface, and atmospheric pressure, leads to the formation of bis(dipyrrinato)zinc(II) laminar complex (**N1**) (Fig. 6).[13] The sheet transferred to SiO_2 substrates *via* Langmuir-Schäfer method shows a height in AFM of 1.2 nm which corresponds to a single layer, while XPS confirms its composition. AFM phase images show domain sizes of the single-layer sheet as large as *ca*. 10 μm. The analysis of the sheet by STM reveals that the layer shows a Moiré pattern composed of two lattices: one is in the in-plane hexagonal periodicity of **N1** and the other is derived from HOPG substrate. Finally, they also proof that repeated deposition of the single-layer sheet **N1** on a flat substrate resulted in its quantitative layering.

Liquid/Liquid interface. This procedure has been only useful to obtain few layers but still no single layers. Therefore, in this section we highlight only those works showing the production of materials with a nanometric thickness.

The reaction between the dipyrrin ligand (**L1**) and zinc(II) acetate carried out at the liquid/liquid interface of a CH_2Cl_2 solution of **L1** and a water solution containing the metal salt produces multilayer bis(dipyrrinato)zinc(II) complex nanosheet (**N1**) (Fig. 7).[13] Interestingly, the thickness of the layers can be controlled varying the concentration of **L1** between 1×10^{-6} to 5×10^{-4} molL^{-1} giving rise to thickness corresponding to 5 to 670 layers (Fig. 7e,f). Selected area electron diffractions (SAEDs) in transmission electron microscopy confirmed the in-plane periodicity of the multilayers. They represent two sets of hexagonal diffractions, which are consistent with in-plane diffraction patterns reproduced from crystal lattices comprising piles of single-layer **N1**, which were optimized using a molecular mechanics calculation.

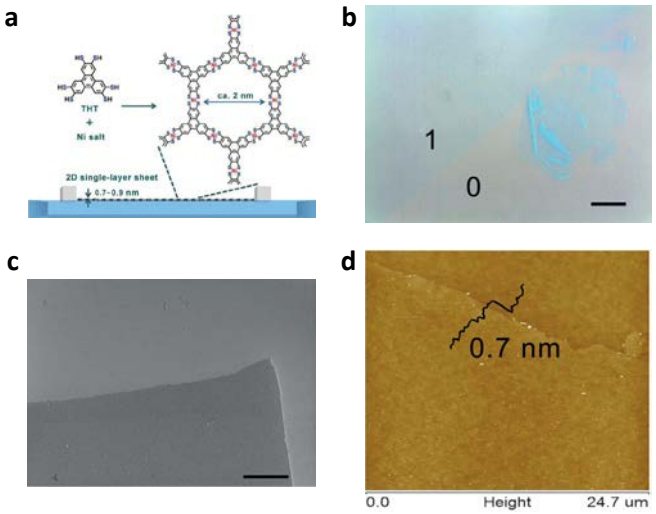

Fig. 5 a) Synthesis of a single-layer sheet coordination polymer based on triphenylene-fused nickel bis(dithiolene) complex by using the Langmuir-Blodgett method at the air/water interface. b) Optical microscopy image showing large-area nickel bis(dithiolene) complex sheets (Scale bar: 100 mm). c) SEM image of a single-layer sheet (Scale bar: 10 mm). d) AFM topographic images and its corresponding height profile showing a single-layer sheet with *ca*. 0.7 nm in thickness. Adapted from Ref. 12 with permission.

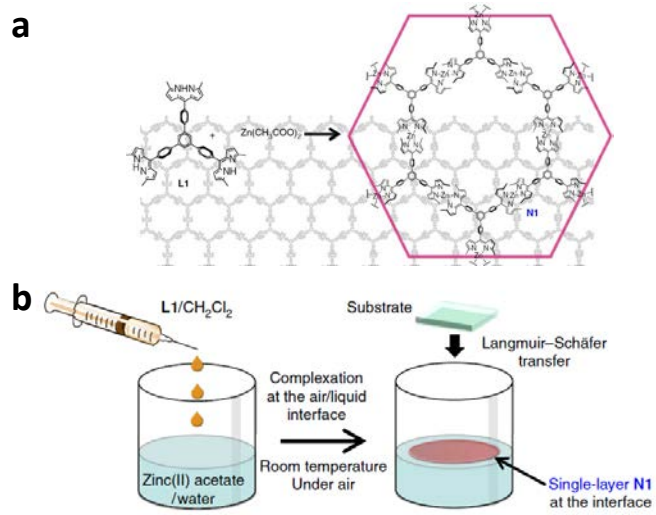

Fig. 6 a) Synthesis and chemical structures of three-way dipyrrin ligand molecule **L1** and bis(dipyrrinato)zinc(II) complex sheet **N1**. b) Schematic sketch of the air/water interfacial synthesis and transfer process. Adapted from Ref. 13 with permission.

The UV-visible spectra of **L1** in toluene and of few-layers **N1** on a quartz substrate shows an intense absorption band at 446 nm for **L1**, which is derived from the $\pi-\pi^*$ transition of the dipyrrin π-system. Complexation with zinc(II) induce a redshift in the $\pi-\pi^*$ transition of *ca*. 49-nm observed in **N1**. Using the $\pi-\pi^*$ band as a probe, single-layer **N1** was accumulated stepwise on a quartz substrate. The single-layer is produced at the air/water interface of a Langmuir–Blodgett trough. The layer can be deposited repetitively on quartz at a constant surface pressure using the Langmuir–Schäfer procedure.

Figure 6b shows the UV-visible spectra of the **N1**-modified quartz substrate. The number of layers deposited on the substrate is proportional to the peak absorbance of the $\pi-\pi^*$ band at 500 nm (Fig. 7e,f).

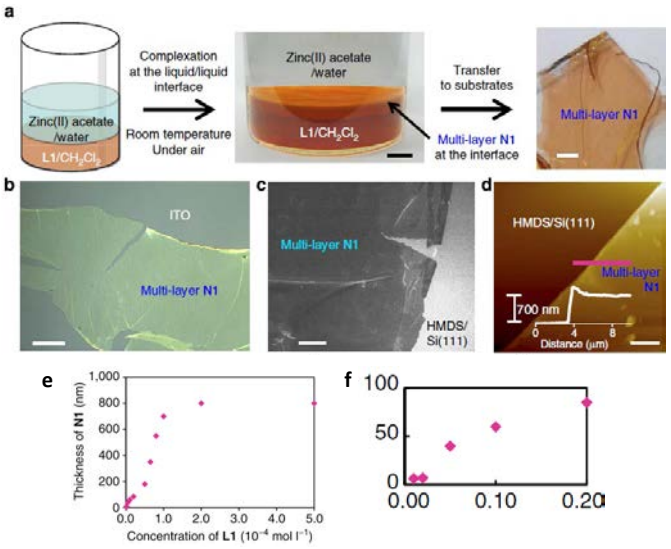

Fig. 7 (a) Illustration and photographs of the liquid/liquid interfacial synthesis and multi-layer **N1** transferred onto an ITO substrate (scale bar 1 mm). (b) Optical microscopic image on an ITO substrate. Scale bar, 50 μm. (c) Field-emission scanning electron microscopic image on 1,1,1,3,3,3-hexamethyldisilazane/Si. Scale bar, 20 μm. (d) Atomic force microscopic image on 1,1,1,3,3,3-hexamethyldisilazane/Si and its height profile along the magenta line. Scale bar, 5 μm. (e) Control of the thickness experiment carried out for 4 days at room temperature using different concentration of **L1**. (f) A close-up of the low concentration region. Figure adapted from Ref. 13 with permission.

In a similar approach *Gascón et al.* have produced MOF nanosheets of Cu(II)-1,4-benzenedicarboxilate (CuBDC) (Fig. 8).[14] They used a strategy that depends on the diffusion-mediated modulation of the MOF growth kinetics. The synthesis medium consists of three liquid layers composed of mixtures of DMF and a suitable miscible co-solvent in appropriate ratios, which are vertically arranged according to their different densities (Fig. 8a). Thus, at the top of a glass sample tube a DMF solution of $Cu(NO_3)_2$ is located, then an intermediate DMF layer, and at the bottom a DMF solution of 1,4-benzenedicarboxylic acid (BDCA). Upon standing at room temperature and static conditions, diffusion of the solutions containing Cu^{2+} and BDCA precursors into the spacer segment causes a slow amount of the MOF building blocks to diffuse to an intermediate region. The SEM and AFM studies of emerging materials separated by sedimentation confirm the formation of square lamellae with lateral dimensions of 0.5-4 μm and thicknesses in the range 5-25 nm (Fig. 8b, c). Interestingly, they observed that the thickness of the CuBDC MOF nanosheets can be modulated by control of the crystal growth kinetics varying the nature of the co-solvent employed and the temperature. X-ray diffraction of the solid products corresponding to the layers of different thickness show just three reflections, which can be assigned to the crystallographic planes of the CuBDC structure, all perpendicular to the stacking direction of the layers in the bulk MOF crystals and to the pore openings. This is indicative of the successful synthesis of structures showing a strong preferential orientation along the basal plane. Finally, a MOF-polymer composite was prepared by incorporation of CuBDC nanosheets within a polyimide matrix and tested as a membrane in the separation of CO_2 (see Properties section 3.1).

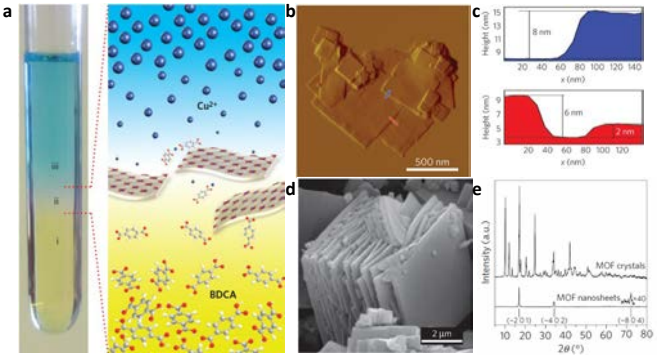

Fig. 8 (a) Glass test tube showing the blue copper(II) salt DFM solution of the top (*iii*), the yellow DMF solution of 1,4-benzenedicarboxylic acid (BDCA) on the bottom (*i*) and the DMF interface were the nanosheets are formed. Topographic AFM image and height profiles (b,c), SEM image (d), and X-ray diffraction peaks (e) of the isolated CuBDC nanosheets. Adapted from Ref. 14 with permission.

Miscellaneous

Direct colloidal formation. Yamauchi *et al.* have synthetized monodisperse 2D-CP nanosheets of $Ni(H_2O)_2[Ni(CN)_4]\cdot xH_2O$ (Ni-CP) through an aqueous solution approach.[15] The nanosheets were directly prepared by mixing at room temperature two water solutions containing $NiCl_2\cdot 6H_2O$ and trisodium citrate dehydrate, with $K_2[Ni(CN)_4]$. A colloidal suspension of well-dispersed Ni-CP nanosheets were obtained upon standing for 24 h. The nanosheets formed present submicrometer lateral dimensions (*ca*. 200×200 μm^2) as was observed using TEM. The crystallinity of the nanosheets was confirmed by wide-angle XRD measurements. A cross sectional SEM image estimated the thickness of the sheets in a range between 5 to 10 nm. Considering that a single layer of Ni-CP should be 0.7 nm in thickness, the obtained sheets appeared to be composed of several stacked layers. The addition of trisodium citrate seems to be a crucial factor for the generation of 2D Ni-CP nanosheets, because it produces a previous coordination between citrate ions and Ni^{2+} ions. This chelating effectively prevented the rapid coordination reaction between Ni^{2+} and $[Ni(CN)_4]^{2-}$ resulting in the deceleration of the crystallization process of Ni-CP. Interestingly the nanosheets were used as a precursor of crystalline nanoporous NiO/Ni nanostructures *via* calcination with high capacitance performances.

Surfactant mediated. Bettina *et al.* have been able to integrate bottom-up with top-down techniques within a chemical setting involving solution processing techniques.[16] This approach is of high interest because is based on a combination of the versatility of "bottom-up" synthesis with the high-precision formation of monodisperse nanostructures by "top-down" delamination. The process uses the surfactant cetyltrimethylammonium bromide (CTAB) as a template to direct the bottom-up synthesis of nanosheets of [Zn(BeIM)OAc] (BeIM= benzimidazole) with an excellent level of size control. This method takes advantage of the lamellar mesophase of the CTAB which is acting as a template for the *in situ* generation of nanosheets. Using CTAB the layered assemblies can be broken up into individual nanosheets easily, as the surfactant layers act as predetermined breaking points and as stabilizing agent preventing the re-aggregation of the nanosheets. In addition, this method involves a single step and hence can be carried out as one-pot reaction. As a result a lamellar hybrid mesostructure is obtained. The hierarchical structure is based on [Zn(BeIM)OAc] nanosheets, with a thickness of *ca*. 2 nm (few layers), covered by the surfactant. The lamellae of the mesostructure are held together by van der Waals interactions between the hybrid material and the CTAB layers. The exfoliation of the multilayer stacks or even individual [Zn(BeIM)OAc] layers was feasible by employing solvent-assisted exfoliation protocols. The exfoliation was carried out using different solvents, being more effective with non-polar solvents, which can penetrate between the hydrophobic interlayer spaces. AFM studies on SiO_2 show that the morphology depends on the solvent used for exfoliation. Thus, regular heights of 10 nm corresponding to a layer composed of CTAB-[Zn(BeIM)OAc]-CTAB were found. Further delamination was possible by additional washing of the surfaces with EtOH to produce nanosheets of 4-7 nm of thickness which are attributed to [Zn(BeIM)OAc]-CTAB and [Zn(BeIM)OAc], respectively.

2.1.2 Covalent Organic Frameworks

Over the past few years, several methodologies have been explored for preparing few-layer covalent organic frameworks and other purely covalent laminar materials using a bottom-up approach.

On-Surface Synthesis. Probably the most straightforward method is casting directly the monomers of the material on a solid substrate so the COF has to grow over the surface, what is known as on-surface synthesis. One of the first successful examples of this approach was reported by Xu *et al.*[17] in 2013, when a monolayer of different imine based COFs was obtained on a HOPG substrate (Fig. 9b). The procedure consists of the deposition of a mixed solution of both monomers on HOPG prior to heating the substrate to favour diffusion of monomers and oligomers, thus allowing a high coverage of the surface and reaction completion (Fig. 9a). Upon study of the samples by STM and AFM, they found single domains of monolayer COF covering over one micron with low density of defects, as could be appreciated in high resolution images (Fig. 9c). This simple method was later applied to grow the same COFs on single-layer graphene,[18] with the potential advantage of allowing transfer between substrates. Very recently it has been demonstrated that using this method it is also possible to prepare COFs with one non-aromatic monomer such as hydrazine or glyoxal;[19] however, as it is expected from the higher flexibility of this molecules, the obtained networks present a higher number of defects.

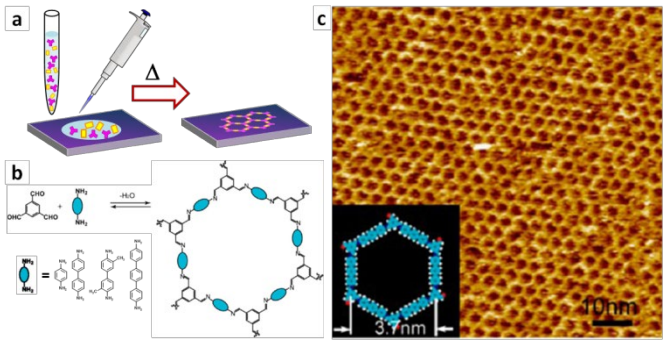

Fig. 9 (a) Scheme of the on-surface interfacial synthesis. (b) Reaction scheme of the formation of hexagonal COFs and backbones represented by the blue ellipse. (c) Large-scale STM image of surface COF, the inset shows the chemical structure of a hexagonal pore of the COF. Adapted from Ref. 17 with permission.

A slightly different approach of the on-surface synthesis gave better results to Liu *et al*.[20] as they obtained nearly defect free single layer areas of 200 nm x 200 nm of two different imine based COFs as shown by STM images (Fig. 10d). They loaded the HOPG substrate with one monomer by drop-casting and put it in a sealed vessel containing the other and more volatile building block.

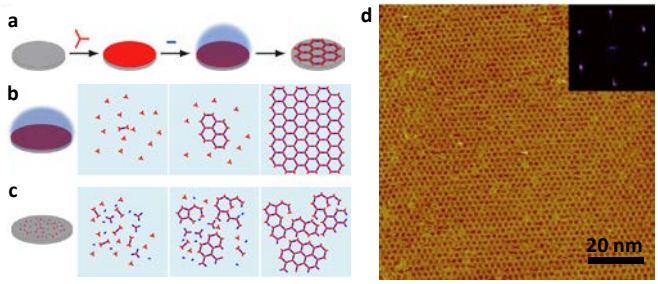

Fig. 10 (a) Scheme diagram for solid-vapour interface synthesis. (b,c) Schematic diagram of the proposed formation mechanism of the COF by solid-vapour interface reaction (b) and by preloading both precursors (c). (d) Large-scale STM image with the inset depicting the corresponding FFT spectrum of the STM image. Adapted from Ref. 20 with permission.

Therefore, when the system is heated, the volatile monomer will vaporize and slowly deposit on the surface, reacting and forming the COF, the presence of a hydrated salt in the reaction medium helps control humidity (Fig. 10a). Under these conditions, the diffusion rate of the vaporized monomer is slow enough to allow reorganization of the oligomers formed on the surface, and the presence of water makes bond formation a reversible process; as a consequence, the majority of errors can be corrected and a highly ordered network is obtained (Fig. 10b). In fact, control experiments were conducted in which the surface was loaded with both monomers, and due to the large number of nuclei formed only small domains were formed (Fig.

10c). The main drawback of this method is the requirement for one of the monomers to be quite volatile, as bigger molecules will decompose before vaporizing.

A big problem of on-surface synthesis is the control over the areas in which the material grows. An interesting solution was reported by Colson *et al*.[21] It was observed that using certain solvent mixtures, a boronate ester COF would selectively grow on graphene instead of over the whole silicon oxide (SiO_2) substrate. Taking advantage of this behaviour, SiO_2 substrates where covered with single layer graphene (SLG) and then the graphene was patterned using lithographic techniques. As expected, when the substrates where immersed in a solution of the building blocks and the typical solvothermal synthesis was carried out, the COF had only grown over the graphene covered areas, reproducing the same pattern that had been lithographed on graphene (Fig. 11a). Grazing incidence X-ray diffraction (GIXD) showed that the COF film had grown with its π-system oriented parallel to single layer graphene; and AFM height analysis proves that the COF only grows over graphene and indicates a minimum film thickness around 40 nm (Fig. 11b-c). Despite being limited by the scarce variety of substrates suitable for this method and the higher thickness of the films prepared, this is a great advance towards real applications as films need to be placed on specific places on devices.

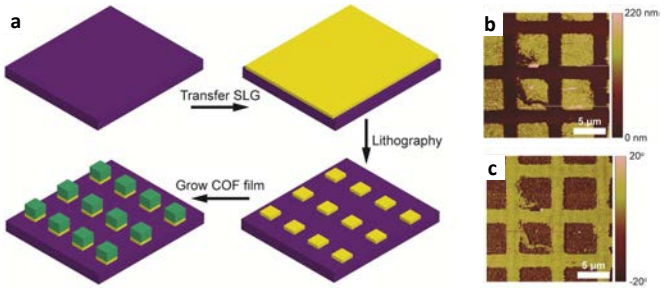

Fig. 11 (a) Scheme of graphene transfer, patterning and subsequent COF growth. (b) AFM height image of COF and its corresponding (c) phase image. Adapted from Ref. 21 with permission.

Another approach for patterning surfaces consists of confining the synthesis in some specific areas of the substrate using very small quantities of solution, as can be done by ink-jet printing or lithographically controlled wetting (LCW) (Fig. 12a).[22] Profiting from the possibility to synthesize an imine-based COF at room temperature and ambient pressure and the ability to control reaction rate, these two techniques were used to pattern both rigid and flexible substrates. Using LCW, stripes 500 nm wide and with thickness below 100 nm were patterned on SiO_2 (Fig. 12b). Better results in terms of height could be obtained using ink-jet printing, as the 10 picoliter droplets expand over a 70 µm diameter circle, the reaction is confined to a smaller height over the substrate and the COF only grows to thicknesses lower than 8 nm (Fig. 12c). Moreover, the printing technique allows patterning a wide variety of substrates (SiO_2, acetate paper) with complex designs.

Air-Liquid Interface. Not only solids provide a surface over which building blocks can be assembled, but the interface between air and a liquid can also be a suitable medium for the growth of two-dimensional structures (see section 2.1.1 bottom up MOFs approach). In fact, liquid surfaces present the advantages of being much flatter than solid ones and as they are completely amorphous the structure of the new material is not affected by the crystalline lattice of the substrate.[2]

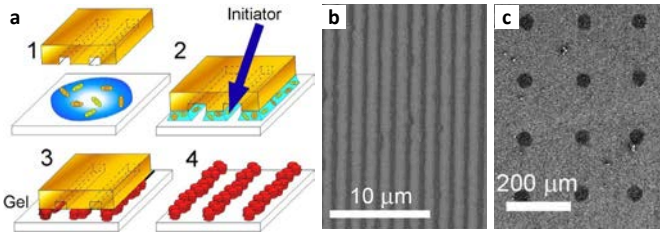

Fig. 12 (a) Scheme of Lithographically Controlled Wetting (LCW) with COF formation in microchannels. (b) Representative FESEM image of 500 nm-in-width COF stripes fabricated by LCW. (c) Representative FESEM image of a 40 µm-in-diameter dot array of COF on flexible acetate paper generated by ink-jet printer. Adapted from Ref. 22 with permission.

A paradigm of the use of the air-water interface was done by Schlüter *et al*.[23] They designed an amphiphilic monomer which would preorganize on the water surface through intermolecular interactions in such a way that would make the anthracene units stack face-to-face (Fig. 13a). This stacking allows that upon irradiation with ultraviolet light a [4+4]-cycloaddition occurs dimerizing the anthracenes and therefore covalently bonding all monomers (Fig. 13a). After polymerization the single molecule thick sheet could be transferred to multiple substrates, making it possible to determine its height as that of a monolayer and equally importantly to check its ability to span over the 20 µm x 20 µm holes of TEM grids; meaning that it can exist as a separate entity from the substrate (Fig. 13b).

A further step towards the synthesis of 2D-polymers using this strategy was taken by Schlüter *et al.*[24] when they were able to prove order in a single layer thick porous film. Using a trypticene core functionalized with three anthraceno blades and a diethylene glycol chain they were able to photopolymerize the film formed at the air-water interface by irradiating it with 365 nm light (Fig. 13a). The 2D-polymer thus obtained was demonstrated to be free-standing in the 20 µm x 20 µm holes of a TEM grid, and can be grown in areas up to 1 mm^2. Moreover, AFM measurements confirm a height of 1.2 nm, corresponding to that of a monolayer, although the most remarkable aspect of this work is the results from STM experiments, which show an ordered material with the expected structure (Fig. 13e).

In the air liquid interface methods other liquids can be used, in a recent work an imine based COF was obtained as thin films from a DMF solution of the monomers.[25] In this case the monomers are not deposited on the interface, instead, after a classical synthesis of COF powder, the resulting solution, which contains the unreacted monomers, is left undisturbed in a water saturated atmosphere and a thin COF film forms spontaneously at the DMF surface. Remarkably, depending on incubation time the thickness of the film could be controlled, ranging 1.8 to 29 nm as measured by AFM.

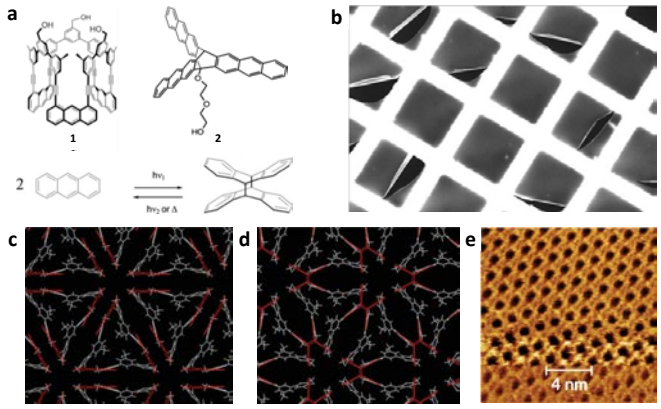

Fig. 13 (a) Structure of the monomers **1** and **2** and scheme of the photopolymerization reaction. (b) SEM image of free-standing 2D-polymer on a TEM grid. (c,d) Structural models of compressed monomer at the interface and the sheet polymer . (e) STM image of sheet polymer. Adapted from Ref. 23 and 24 with permission.

On-solution synthesis. Finally, the last example of bottom-up methodologies consists of the direct synthesis of single and few-layer films suspended in solution.[26] To achieve this, a laminar boronate ester COF was designed in which aromatic rings would not be able to establish π-π interactions between layers; additionally, the triptycene units employed to obtain this geometry were capped with methyl groups to further reduce interlayer interactions (Fig. 14a). All this results in sheets with a low tendency to stack, so when they start to grow in solution, they do not aggregate and if the suspension is pipetted on a substrate, thin sheets of COF can be found, some of them even of single layer thickness (Fig. 14b).

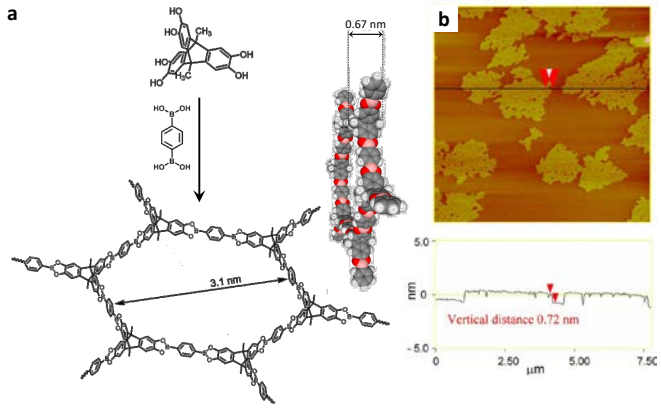

Fig. 14. (a) Structure of the monomer and polymer and scheme of the synthesis. (b) AFM height image of single layer sheets of COF. Adapted from Ref. 26 with permission.

2.2 Top-down

The most common strategies so far used to delaminate layered materials are those based on either micromechanical exfoliation (MME) or liquid phase exfoliation (LPE) (Fig.1). The delamination processes involve the application of mechanical forces to a layered crystal with the corresponding disintegration of bulk material into single- or multi-layers with large lateral dimensions, as large as possible and with the smallest thickness.

There are few efficient approaches for delamination. When the exfoliation is made in solid state we find micromechanical exfoliation (so-called Scotch tape method) and mechanical grinding. Both methods seem efficient ways to produce cleanest, highly crystalline and atomically thin sheets of a layered material. However MME has a clear limitation in the control of the thickness of the materials so-produced as well as a limited production or surface coverage upon stamping on a given substrate.

Therefore, the most common alternative procedure is LPE which is a straightforward, low cost, and high throughput approach. This strategy has been largely developed for many purely inorganic materials, and recently revised by Colleman *et al*.[5] but still little used for COFs/MOFs. This method is based on the sonication, at room temperature, of laminar crystals of COFs/MOFs in a given organic solvent to generate a stable suspension. The solvent selection is not trivial and its selection is related to the structural characteristic of the sample. The adjustment of sonication parameters (power and time) has influence in thickness and lateral dimension of the nanosheets. However, the main problem is to find the appropriate conditions to get either single layers or few layers but with large enough lateral dimensions in comparison to the thickness. The long-range periodicity should not be very much affected in order to keep their structural integrity.

2.2.1 Metal-Organic Frameworks

Liquid phase exfoliation. Crystals of the layered MOF $[Cu_2Br(IN)_2]_n$ (IN= isonicotinate) show weak interlaminar interactions due to the up and down bromide location (Fig. 15a). LPE assisted by ultrasound was successfully used to delaminate these crystals and produce a colloidal suspension in CH_2Cl_2.[27] The drop-casting deposition of this suspension on HOPG shows very homogeneous flakes of 0.5 nm in height and over micron lateral dimensions (Fig. 15b, c). This result agrees with the isolation of single layers of $[Cu_2Br(IN)_2]_n$. X-ray photoelectron spectroscopy (XPS) was used to confirm the structural and chemical integrity of the exfoliated material deposited on surface.

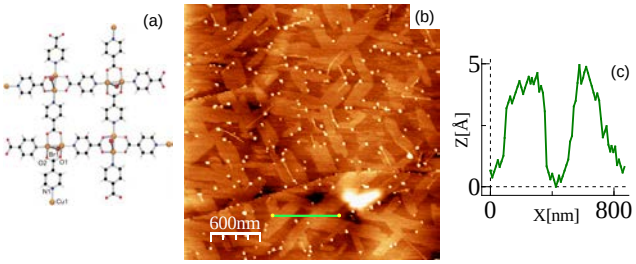

Fig. 15 (a) Structure of a single layer of $[Cu_2Br(IN)_2]_n$. (b) A representative AFM topography image of $[Cu_2Br(IN)_2]_n$ deposited on HOPG, and (c) its height profile across the green line in (b). Reproduced from Ref. 27 with permission.

Later Tang Q *et al.*,[28] carried out theoretical studies on the electronic and magnetic properties of a monolayer of $[Cu_2Br(IN)_2]_n$, and investigated its interactions with different gases to explore the feasibility of using single layers of $[Cu_2Br(IN)_2]_n$ as a molecular sensor. Among the several gases tested, NO and NO_2 showed the stronger

interactions with modification of the electronic structure of the monolayer. Therefore, these studies suggest the viability to prepare ultra-sensible sensors based on the use of single layers of a MOF.

A related neutral MOF, $\{Zn(TPA)(H_2O)\cdot DMF\}_n$ (TPA= terephtalic acid), has also been delaminated *via* LPE assisted by ultrasonication of the corresponding bulk crystals in acetone.[29] Additionally, these nanosheets showed a remarkable amine intercalation, leading to re-stacking, and reversible amine exchangeability.

Cheetam *et al*.[30] have described the production of nanosheets from dense non-porous CPs *via* LPE assisted by ultrasound with a variable thickness ranging from single to many layers. The starting layered crystals are based on Mn(2,2-DMS) (2,2-DMS= 2,2-dimethylsuccinate) in which the layers are held together by weak van der Waals interactions. This work suggests that the use of non-porous and dense CPs instead of MOFs seems to be more straightforward due to the fact that non-porous structures are inherently more robust, allowing to characterize the material by electron diffraction (despite the thickness of the sheets used in these characterization experiments is not completely clear). Additionally, indentation experiments allow an estimation of the mechanical properties of the isolated multilayers (*ca*. 50 layers) of 6-7 GPa. In a following work the same authors have explored the exfoliation of different structures of 2,2´-DMS with several cations (Li, Co, Zn).[31] The topologies of the layers in each CP differ and this seems to have a significant consequence on the relative size of the nanosheets formed. But unlike MnDMS, which can be exfoliated to a level of single layers, for the rest of cations the smallest thickness exceeds 10 layers. The lateral dimensions of the series of exfoliated nanosheets compared to thickness tends to decrease in the order LiDMS > MnDMS > ZnDMS. The results suggests that factors such as the extent of inorganic connectivity and the space between neighbouring methyl groups produce the formation of thin nanosheets with larger lateral dimensions.[31]

In an extension of this research work, the same authors have studied the preparation and LPE assisted by ultrasound of a series of dense layered CPs with the 2,3-dimethylsuccinate ligand (2,3-DMS) and Mn, Co or Zn as cations.[32] They observed an ease exfoliation of the layered frameworks M(2,3-DMS) suggesting that these layered CPs are more corrugated than their M(2,2-DMS) analogous, therefore exfoliating more rapidly. Importantly, powder diffraction patterns were obtained from the nanosheets collected by centrifugation of the suspensions, confirming that the reconstituted materials show almost the same crystal structure as the bulk. This suggests that LPE does not produce significant changes in the layer structure of these materials. Despite the fact that they could isolate and characterize nanosheets with a thickness close to the single layer level, the lateral dimensions were limited to 500-50 nm, while multilayers (thickness *ca*. 100 nm) were isolated with much larger lateral dimensions (10 x 10 μm^2).

Kitagawa *et al*.[33] have studied the solvothermal synthesis and the LPE of a laminar MOF Cu–TCPP [TCPP = 5,10,15,20-tetrakis(4-carboxyphenyl)porphyrin]. The as-synthetized material presents a laminar structure as it is clearly showed by SEM images. The sonication of the bulk Cu–TCPP in ethanol or acetone produces a dispersion of nanosheets without any curling. The TEM images of the nanosheets isolated from the suspension show a quite homogeneous material with lateral dimensions of *ca*. 200×200 nm^2 (Fig. 16a, b). The analysis of the AFM images confirms a very uniform thickness of *ca*. 15 nm. Using this suspension, the authors have developed a novel modular assembly concept, using the Cu–TCPP nanosheets as modules for assembly into a MOF thin film by a simple transfer stamping process. The "modular" process starts with the nanosheet suspension which is deposited dropwise onto the surface of water in a beaker, which acts as a flat substrate, and the hydrophobic nature of the Cu–TCPP nanosheets allows them to spontaneously spread out to form a thin film; finally, the thin film can be transferred to a solid substrate by stamping (Fig. 16 c, d). Using this stamping procedure, a layer-by-layer growth model was used to produce MOF thin films with controlled thickness. X-ray analysis demonstrated that the stamped films are highly crystalline and oriented. Therefore, this novel and simple approach seems to be suitable for preparing highly oriented crystalline thin films of MOFs that cannot be prepared by traditional techniques.

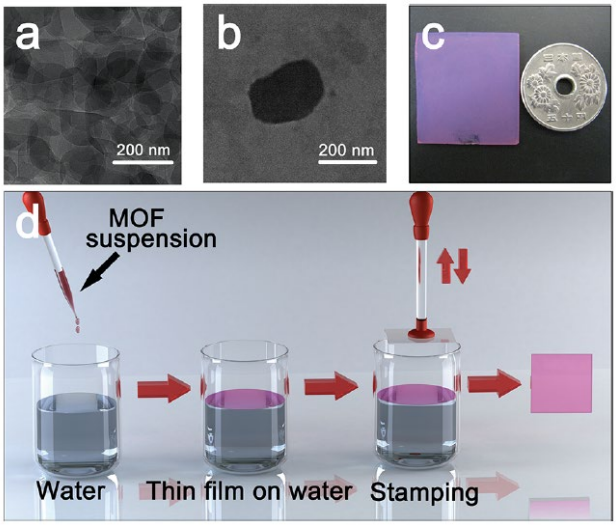

Fig. 16 (a, b) TEM images of the dispersed Cu–TCPP nanosheets. (c) Photograph of the MOF thin film after 15 deposition cycles on a quartz substrate. (d) Schematic illustration of the assembly process. Reproduced from Ref. 33 with permission.

As already mentioned the use of sonication has some clear limitations in size, thickness *vs* lateral dimensions, but also in the possibility to induce in plane structural defects. In order to avoid this problem Zamora *et al*.[34] synthesized a new 2D-MOF $[Cu(\mu\text{-}pym_2S_2)(\mu\text{-}Cl)]_n$ nH_2O (pym_2S_2=dipyrimidinedisulfide) which shows weak interlaminar interactions as well as cavities, in which molecules of solvent are located. Just by immersion of crystals of this MOF in water the material was fully delaminated after 4 days (Fig. 17 a, b). The single-layers produced in water suspension were isolated on several surfaces and characterized by AFM (Fig. 17c, d) as well as XPS.

The lateral dimensions of the isolated single layers range between *ca*. 200×200 nm^2 to 1×1 μm^2. This unprecedented observation is a direct consequence of the solvent in the crystal network which prevents strong layer to layer interactions and

by the interlayer cavities that can be filled by the solvent molecules producing delamination in a simple way. Additionally, using much larger crystals and LPE assisted by sonication, $[Cu(\mu\text{-}pym_2S_2)(\mu\text{-}Cl)]_n$ were delaminated in water to produce flakes with areas of hundreds of square microns with an excellent control of the molecular thickness (from single up to *ca*. 50 layers). These outstanding morphological features allowed further physical characterization of the isolated layers that exhibit good photoluminescence and mechanical properties as to allow free-standing characterization of few layers' flakes (see results in Section 3).[35]

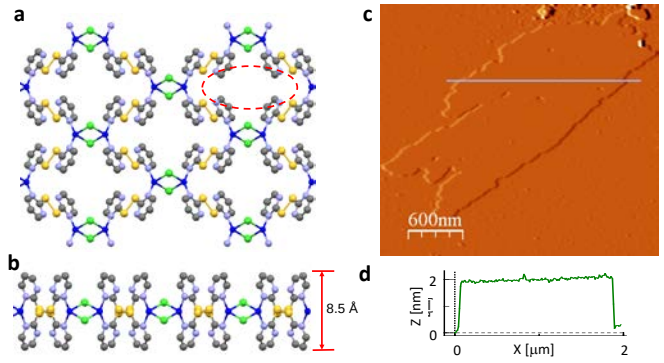

Fig. 17 (a) View of a layer of $[Cu(\mu\text{-}pym_2S_2)(\mu\text{-}Cl)]_n$ nH_2O with a cavity were the solvent is located market in red and (b) a lateral view of this layer with an estimation of its thickness. Topographic AFM image of a typical single layer of $[Cu(\mu\text{-}pym_2S_2)(\mu\text{-}Cl)]_n$ nH_2O and its height profile (d). Adapted from Ref. 34 with permission.

Similarly, the exfoliation of a lanthanum 1,3,5-benzenetriphosphonate 2D system (LBP-II) takes place just by shaking the crystals in dimethyl formamide. The structure of LBP-II consists of layers with chains of lanthanide bridged by phosphonates stacked by hydrogen bonds and van der Waals interactions, therefore the interaction with polar solvents is favoured. As a result LPE allowed the isolation of nanosheets with a minimum thickness of 1.3 nm by AFM, which corresponds to single layer of a lanthanum 1,3,5-benzenetriphosphonate 2D system.[36] However, the observed lateral dimensions of the isolated nanosheet are rather poly-dispersed and very small (*ca*. tens of square-nanometers). Importantly, X-ray powder diffraction of the solid isolated from the suspension supports that the structure of LBP-II is retained after exfoliation.

W. Yang *et al*.[37] have recently reported the efficient exfoliation of the layered MOF poly[Zn_2(benzimidazole)$_4$], named as $Zn_2(bim)_4$, based on a two-step procedure. First, pristine $Zn_2(bim)_4$ crystals were wet ball-milled at low speed (60 rpm) and, second LPE in volatile solvent assisted by ultrasonication. They found that a mixture of methanol and propanol is the most suitable for exfoliation. They suggest that wet ball-milling facilitates the penetration of small methanol molecules into the galleries of the layered $Zn_2(bim)_4$, and propanol helps to stabilize the exfoliated nanosheets by adsorbing on the sheets with its hydrophobic alkane tails. AFM images confirm large lateral dimension up to 1.5 μm and a uniform thickness of 1.12 nm consistent with a single layer.

Micromechanical exfoliation. Coronado *et al*.,[38] have presented the first examples of micromechanical exfoliation from bimetallic complexes based on anilate (An) bis-bidentate bridging ligands. In this work they carried out a comparative study between the micromechanical exfoliation of neutral layers of the CPs based on $[Fe^{III}(acac_2\text{-}trien)]$ $[Mn^{II}Cr^{III}(Br_2An)_3].(CH_3CN)_2$ and LPE. The layers in the crystal are hold by weak van der Waals forces which facilitate both mechanical Scotch tape and LPE. The final results obtained by micromechanical exfoliation agree with a level of exfoliation of single layers (apparent height in AFM of 2 nm on SiO_2), however with a high dispersion of thickness. Additionally, they showed similar results for the case of the analogous ionic layered anilate-based compound $[Fe^{III}(sal_2\text{-}trien)][Mn^{II}Cr^{III}(Cl_2An)_3]\cdot solv$ (solv= several solvents) whose structure is formed by alternating anionic layers. However, LPE of the ionic layered material is hindered giving rise to a lower level of exfoliation to that obtained with the neutral counterpart. This is likely due to the stronger ionic interactions between the layers. Another general observation is that the use of LPE method reduces the lateral size of the sheets from micro to few hundred nanometers in comparison to those obtained by micromechanical exfoliation.

2.2.2 Covalent Organic Frameworks

Purely organic materials can also be exfoliated in a top-down approach. Although they are most commonly used, ultrasounds are not the only option, as we will see in this section.

Liquid phase exfoliation. Although the structures of many COFs heavily resemble that of graphene, it is not possible to use micromechanical exfoliation due to the small size of all the crystals of laminar COF synthesized up to date. Therefore, other methods have been applied to overcome this difficulty. The first attempts to use ultrasounds to exfoliate COF powders were reported by Zamora's group. In a first study, a boronate ester COF was synthesized and the resulting powder was sonicated and adsorbed on substrates.[39] XPS characterization showed that no decomposition had taken place and analysis of the AFM images confirmed that 10-layer thick sheets were obtained. In a more systematic study, a family of conjugated microporous polymers (CMPs) with different pore sizes, was sonicated for a series of different times, and after studying the minimum thickness of each CMP it could be established that those with smaller pore diameter could be delaminated to lower thicknesses (Fig. 18).[40]

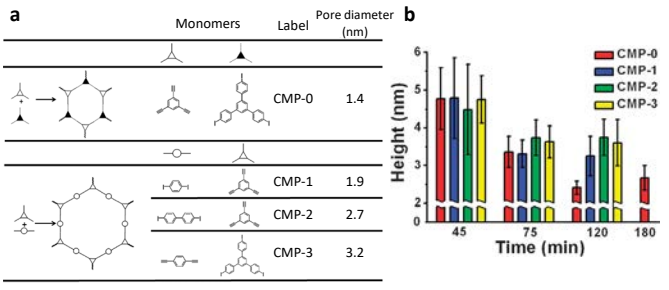

Fig. 18 (a) Description of the layered polymers studied. (b) Histograms of relative height for CMP nanosheets after sonication at different times. Adapted from Ref. 40 with permission.

The last example of the use of ultrasounds that is going to be discussed focuses on the interaction of solvents with a hydrazone based COF (named as COF-43).[41] The loss of crystallinity observed when COF-43 powder is soaked in some solvents is correlated with the higher ability of these solvents (e. g. dioxane, water or DMF) to generate thinner sheets, as it is suggested that it is exfoliation which causes the disappearance of diffraction peaks, even if it does not provoke covalent bond breakage. Combining the action of the solvent with some sonication, it was possible to reach thicknesses of 1.3 nm using dioxane.

Exfoliation by mechanical grinding. A widely recognized drawback of the use of ultrasounds is that they can induce the creation of defects in the structure of the exfoliated sheets. Another approach to deal with microcrystalline powders that does not use sonication was reported by Chandra *et al.*[42] In this work, five different imine based COFs were ground in a mortar with a few drops of methanol. The study of the resulting material by TEM and AFM showed the presence of layered sheets with thickness in the range of 3-10 nm.

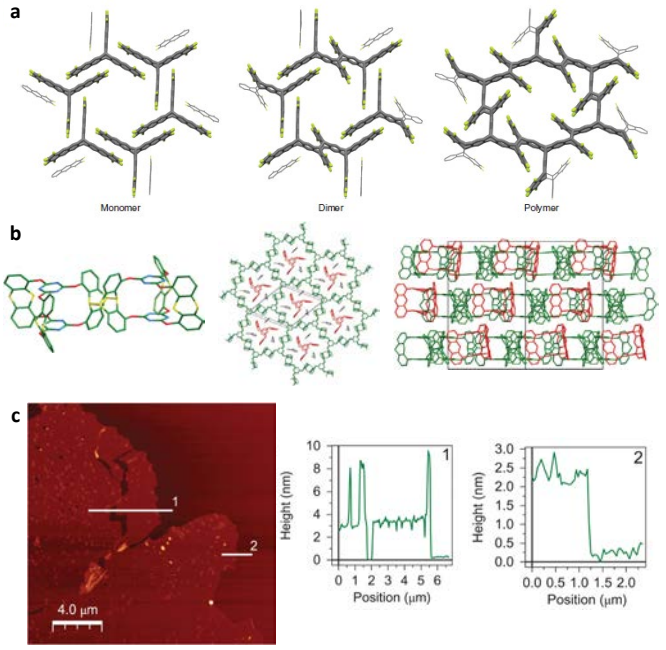

Fig. 19 (a) X-ray crystal structures of the fantrip monomer, fantrip dimer and poly(fantrip) (From Ref. [43]). (b) X-ray crystal structures showing two connected anthracene blades with the new bonds in yellow; top and side view of the polymer sheet, the colour code reflects whether the three bladed compound acts as monomer (green) or template (red) (From Ref. [44]). (c) AFM image of a 30 μm sheet composed of three stacked layers, and corresponding height profiles. Adapted from Refs. 44 and 43 with permission.

Crystal-to-crystal synthesis. The necessity to use the previous techniques arises from the lack of single crystals with an appropriate size. In 2014, Schluter's[44] and King's[43] groups simultaneously reported the syntheses of single crystals of covalently bonded layered materials. Both groups followed the same approach; they synthesized a monomer that would be prone to crystallize in a geometry in which their anthracene units would stack face-to-face, thus allowing to polymerize them by irradiation with UV light (Fig. 19a, b). As the [4+4]-cycloaddition does not imply significant displacements of the atoms, just a rearrangement of the electrons, the monomer crystals polymerize without breaking affording polymer crystals of the same size. So far, the only attempts to isolate single-layers of from these crystals have resorted to ultrasounds, resulting in 3nm thick sheets (Fig. 19c-e). However, the possibility of synthesizing crystals of these materials, opens up the option of using micromechanical exfoliation to obtain high-quality, defect-free films of 2D covalent polymers.

3. Properties

3.1 Metal-Organic Frameworks

In a seminal work on the analysis of the properties of single layers of MOFs, the suspensions of single/few layers of 1,3,5-benzenetriphosphonate (LBP-II) with Tb(III) and Eu(III) show photoluminescence in green and red, respectively (section 2.1.2 MOFs, LPE). The broad emission bands at 230 and 268 nm are due to ligand to metal charge transfer (LMCT) from phenyl groups of 1,3,5-benzenetriphosphonate (BTP), which is supported by the UV-vis spectrum of HBTP.[36] The emission and excitation spectra of nanosheets are similar to those of the bulk one.

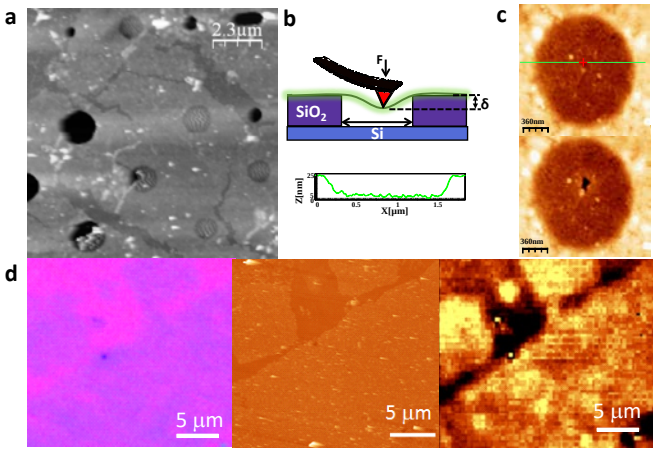

Fig. 20 (a) Morphological characterization of free-standing the layers of $[Cu(\mu\text{-}pym_2S_2)(\mu\text{-}Cl)]_n{\cdot}nMeOH$ obtained on Si/SiO_2 (300 nm) substrates with wells. (b) Schematic representation of nanoindentation experiment on suspended MOF membrane. (c) Dynamic mode AFM image of a covered hole (1 μm in diameter) by $[Cu(\mu\text{-}pym_2S_2)(\mu\text{-}Cl)]_n{\cdot}nMeOH$ membrane and a fractured membrane from indentation. (d) Optical image (left) and AFM topographic image (middle) of a large flake of $[Cu(\mu\text{-}pym_2S_2)(\mu\text{-}Cl)]_n{\cdot}nMeOH$ on SiO_2, respectively, and confocal image (right) of flakes of $[Cu(\mu\text{-}pym2S2)(\mu\text{-}Cl)]_n{\cdot}nMeOH$ on an Si/SiO_2 substrate. The colour-scale reflects the intensity within a Raman shift of 100 cm^{-1} from the elastically scattered light, i.e., the image represents reflected light. Adapted from Ref. 35 with permission.

The large lateral dimensions of the single to few layers of the MOF $[Cu(\mu\text{-}pym_2S_2)(\mu\text{-}Cl)]_n$ isolated on SiO_2 have allowed the characterization of their mechanical properties and photoluminescence in detail. Indeed, it was possible to isolate free-standing few layer flakes (Fig. 20a) which were suitable to perform a full study on its mechanical properties. The values obtained show a Young's modulus of 5±0.5 GPa and a breaking forces of about 40 nN ($\sigma^* = 1 \pm 0.4$ GPa). This Young's modulus is

the lowest reported so far. Mechanical stability is a relevant topic for 2D materials due to the mechanical properties are sensitive to defects and thus they can be used as an indicator for the structural integrity and stability of the layers towards their potential applications and device fabrication.[45] The comparison of the PL-Raman spectra of isolated single *vs* few layers (Fig. 20 d) and the comparison with the emission spectra of the bulk material show a significant red shift of the emission from single to few to bulk.[35]

As previously mentioned the nanosheets of Cu(II)-1,4-benzenedicarboxilate (CuBDC) were used to prepared a composite material with a polyimide matrix (PI).[14] The structural characterization of the composite by FIB-SEM tomograms reveals the freestanding and dispersible nature of the CuBDC nanosheets (Fig. 21). The CuBDC-PI composite was cast as thin membranes with thickness ranging between 30-50 μm. It is remarkable that the image analysis shows that the CuBDC nanosheets in the composite there is a significant larger occupation of the membrane cross section perpendicular as compared to the isotropic monocrystals of CuBDC embedded in PI. This preferential orientation of the nanosheets allows the gas flux through the molecular sieve, increasing the probability of repeated molecule discrimination events and efficiently eliminating MOF-free diffusion pathways.

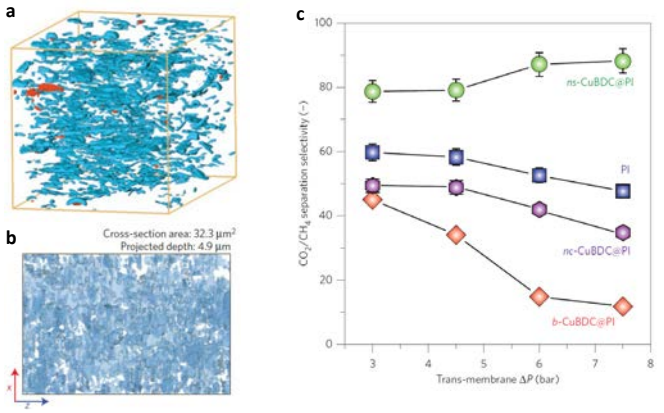

Fig. 21 Tomographic FIB–SEM analysis of CuBDC–PI composite membrane showing a surface-rendered view of the segmented FIB–SEM tomograms (a) and a full projection along the *y* direction of the reconstructed volume for composite membranes. Adapted from Ref. 14 with permission.

As a result, the incorporation of MOF nanosheets into PI provides exceptional CO_2 separation performance from CO_2/CH_4 gas mixtures, together with an unusual and highly desired enhancement in the separation selectivity with pressure (Fig. 21). These results suggest potential applications for MOF nanosheet-polymer composites.

Similarly, the nanosheets of the layered MOF $Zn_2(bim)_4$ were used as building blocks for ultrathin molecular sieve membranes (Fig. 22). A hot-drop coating process was used to produce a disordered stacking of the nanosheets in the membrane layer. Thus a diluted methanol suspension of nanosheets of $Zn_2(bim)_4$ was deposited dropwise onto the surface of an α-Al_2O_3 disk which was heated at 120°C on a heating plate to produce an uniform surface coverage of $Zn_2(bim)_4$ nanosheets on α-Al_2O_3. These membranes show hydrogen gas permeance of up to several thousand gas permeation units (GPUs) with H_2/CO_2 selectivity greater than 200. An unusual proportional relationship between H_2 permeance and H_2 selectivity for the membranes, and achieved a simultaneous increase in both permeance and selectivity by suppressing lamellar stacking of the nanosheets.[37]

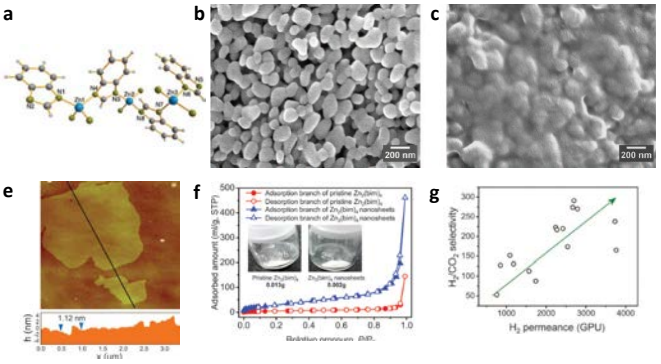

Fig. 22 (a) Representation of the repetition unit of $Zn_2(bim)_4$ (b) SEM image of a bare porous α-Al_2O_3 support. (c) SEM top view. (e) Tapping mode AFM topographical image of $Zn_2(bim)_4$ nanosheets on silicon. The height profile of the nanosheets along the black lines was marked in the image showing isolation of single layers. (f) N_2 adsorption-desorption isotherms (77 K) on pristine $Zn_2(bim)_4$ and $Zn_2(bim)_4$ nanosheets. The inset presents photographs comparing the pristine $Zn_2(bim)_4$ and $Zn_2(bim)_4$ nanosheets obtained after exfoliation. (g) Anomalous relationship between selectivity and permeance measured from 15 membranes. Adapted from Ref. 37 with permission.

The nanosheets of bis(dipyrrinato)zinc(II) complex (**N1**) show several interesting properties.[13] On the other hand, they show the ability to uptake the fluorescent dye, Rhodamine B, into the large pores of **N1** upon immersing multi-layer **N1** on an ITO or quartz substrate in a CH_2Cl_2 solution of Rhodamine B. Guest-incorporated **N1** showed fluorescence from Rhodamine B. Additionally, multi-layers of **N1** deposited on a SnO_2 electrode functions as a photoanode in a photoelectric conversion system, and is the first photofunctional bottom-up nanosheet.[13] The nanosheets collect visible light on transparent SnO_2 operated as an active layer, working as a photoanode, in a photoelectric conversion system (Fig. 23). Indeed this is a very promising photofunctionality of a molecule-based bottom-up nanosheet towards potential application in optoelectric conversion devices.

It is well-known that complexes based on π-conjugated metal bis(dithiolene) are active sites of molecular catalysis for photocatalytic and electrocatalytic hydrogen generation from water. Therefore, the electrocatalytic activity of the single-layer sheet of nickel bis(dithiolene) above commented was evaluated. Interestingly, the nanosheets deposited on rotating disk electrode (RDE) in an argon-saturated aqueous solution show outstanding electrocatalytic activities for hydrogen generation from water with a Tafel slope of 80.5 $mVdecade^{-1}$ and an overpotential of 333 mV at 10 $mAcm^{-2}$.[12] These values indicate that the nanosheets are highly efficient in the electrocatalytic hydrogen evolution reaction (HER) with values even higher to those found for carbon nanotube supported molecular catalysts and heteroatom-doped graphene catalysts.

This work highlights the promising potential of free-standing metal-organic 2D materials for energy technologies.

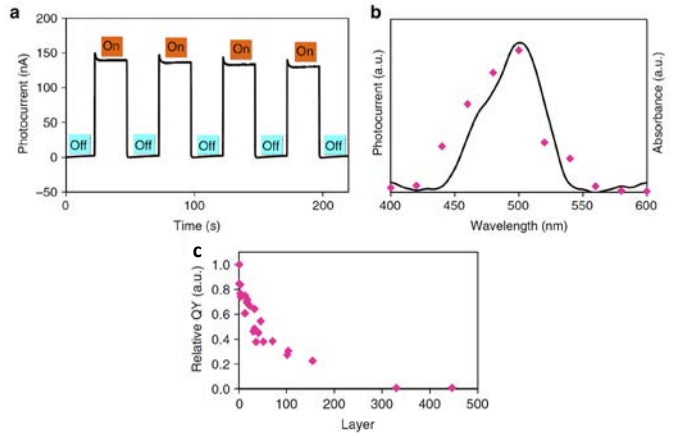

Fig. 23 (a) Anodic current response on irradiation with intermittent 500-nm light of a working electrode of SnO_2 modified with 36-layer **N1**. (b) Spectrum for the photocurrent generation (magenta dots) and absorption spectrum of **N1** (black solid line). (c) Relationship between the relative quantum yield (QY) and thickness of **N1** on irradiation with 500-nm light. The highest QY (0.86% by single-layer **N1**) is taken as the standard. Adapted from Ref. 13 with permission.

3.2 Covalent Organic Frameworks

Due to the reduced number of tested applications of 2D COFs, in this section we are also going to include some works in which the materials have thicknesses above 100 nm, in order to show some potential applications.

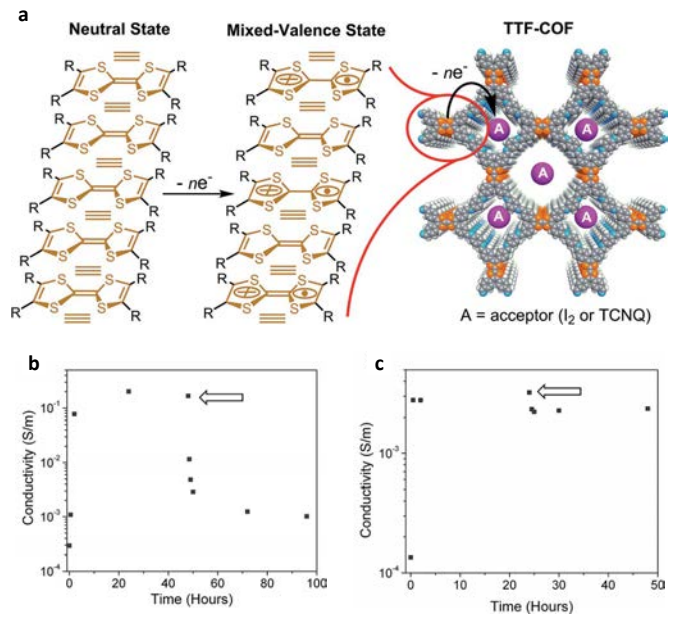

Fig. 24 (a) Illustration of the mixed-valence state of TTF-COF. (b,c) Time dependent conductivity changes of TTF-COF thin films upon exposure to I_2 and TCNQ, respectively. The arrows indicate the time of the thin films being removed from doping environments and kept in open air. Adapted from Ref. 46 with permission.

In the first example an imine based COF containing tetrathiofulvalene (TTF) units is synthesized directly over SiO_2 substrates with gold electrodes (Fig. 24a).[46] A 150 nm thick film of COF layers oriented parallel to the substrate is obtained, which shows a conductivity of 10^{-4} S m^{-1}. The films were exposed to iodine vapours or tetracyanoquinodimethane (TCNQ) solutions to partially oxidize TTF units in order to increase conductivity of the COF, reaching values up to 0.3 S m^{-1} and 3 x 10^{-3} m S^{-1} respectively (Fig. 24b, c). Moreover, the conductivity can be tuned depending on the adsorption time of the dopants.

In another work, Medina *et al.* functionalized a boronate ester COF with fullerenes to test its performance in charge transfer processes (Fig. 25a).[47] To this purpose, the COF was designed with benzodithiophene (BDT) units that would act as donors, while the fullerenes would be the acceptors (BDT-COF, BDT-COF [60]PCBM and BDT-COF [70]PCBM).

The direct synthesis of the COF on ITO or NiO covered ITO yielded a film oriented parallel to the substrate and with thickness of 150 nm (Fig. 25). Fluorescence studies and femtosecond spectroscopy confirmed formation of polarons and charge transfer from the COF to fullerenes (Fig. 25c-d).

Finally, the last example, which was already discussed in the bottom-up section (2.1.2 COFs), uses a 5 nm thick film as a field-effect transistor (FET) (Fig. 26).[25] The device was built using the COF film as semiconductor over a Si/SiO_2 substrate with gold contacts. Even if the experiments measured an on/off ratio of 850 and low charge carrier mobility (3 x 10^{-6} cm^2 V^{-1} s^{-1}), they still demonstrated its behaviour as a FET, which means that this thin film can be used to build real devices.

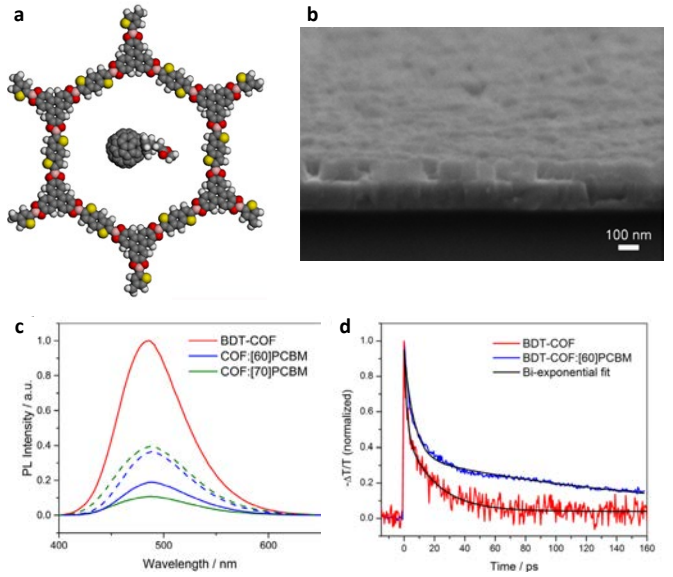

Fig. 25 (a) Scheme of the structure of BDT-COF [60]PCBM. (b) SEM micrograph in cross section of BDT-COF thin film grown on an ITO-coated glass substrate. (c) Photoluminescence spectra of films of BDT-COF without and with fullerenes. (d) Femtosecond pump-probe transient absorption measurements of hole-polaron lifetime. Adapted from Ref. 47 with permission.

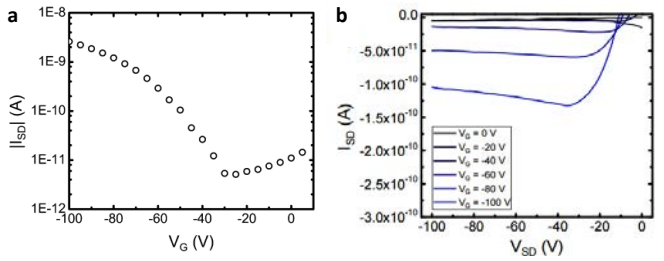

Fig 26. (a) Transfer plot of thin-film transistor employing COF film active layer. (b) Output plot of a COF based transistor. Taken from Ref. 25 with permission.

Conclusions

2D-polymers is still a relatively new scientific field which is essentially dominated by graphene and its family. This family includes mainly selected allotropic forms of some elements, including carbon as graphene phosphorous as black phosphorous, and binary combinations such as BN besides combinations of transition metals with sulphide, like MoS_2, and halides. Even 10 years after the discovery of graphene, this group continues to grow with the incorporation of new members.

However, in addition to this purely inorganic list of materials that lack structural design, this feature article attempts to show the opportunities that synthetic chemistry can bring to the this emerging field. Indeed, the number of samples reported using chemical synthesis is very limited but promising. We have focused on 2D-polymers based on metal-organic and purely organic chemically designed materials, specifically those based on MOFs and COFs, but nevertheless other designed materials will become relevant as for instance Layered Double Hydroxides.[48]

The information here collected shows that, during the last few (3-4) years, the evolution in preparation of 2D-polymers has clearly evolved from the initial samples using the top-down delamination approach, to new bottom-up methods that have allowed the production of 2D-polymers with ultra-large areas close to square centimetres. Therefore, novel synthetic methods and the refinement of the already known should provide a better control of thickness versus lateral dimensions. In the next coming years we will probably see the incorporation of new procedures, probably including Chemical Vapour Deposition, in order to provide alternatives and overcome some of the limitations and problems of the already known methodologies. The increasing availability of more powerful techniques at the nanoscale level such as scanning electron and probe microscopies, as well as spectroscopic and diffractometric techniques has fuelled the blossom of studies devoted to the isolation of 2D crystallites. Obviously, one of the most outstanding developments of the isolated layers of both MOFs and COFs is their evolution from merely preparatory aspects to the evaluation of the physico-chemical properties. This is an essential aspect towards the fabrication of the first prototype devices. Indeed, in this manuscript we have shown layers showing catalytic activity, light emission, gas adsorption at the level of nanosheets. The confirmation of these properties enables the use of these materials in potential applications for gas separation membranes, ultrasensitive molecular sensors, novel catalysis and new materials for energy production. Some of these properties are consequence of the thickness reduction, for instance gas separation is dramatically enhanced in a polymer composite based in the use of MOF nanosheets,[14] photoelectric conversion or electrocatalytic hydrogen evolution.[12]

We are sure that the approach based on the use of chemistry for 2D-polymer preparation will spread in parallel to 2D-polymers based on many more different materials (metallic carbides, pure elements, ….). Additionally, new materials based on the controlled stacking of layers of different materials including graphene-family with layers of COFs/MOFs will produce new hybrids useful for device fabrication with unprecedented functionalities. However, despite we envision a great future for 2D polymers, it still seems too early to conclude whether or not 2D polymers will be present in future technology, although the recent findings shown in this manuscript suggest that their influence will be evident in the immediate future.

Acknowledgements

Financial support from Spanish MINECO (MAT2013-46753-C2-1-P and MAT2013-46502-C2-2-P). D. R. thanks the Spanish MECD for a FPU grant.

Notes and references

1. J. Sakamoto, J. van Heijst, O. Lukin and A. D. Schluter, *Angewandte Chemie-International Edition*, 2009, **48**, 1030-1069.
2. P. Payamyar, B. T. King, H. C. Ottinger and A. D. Schluter, *Chem. Commun.*, 2015, in press. DOI: 10.1039/C5CC07381B.
3. K. S. Novoselov, A. K. Geim, S. V. Morozov, D. Jiang, Y. Zhang, S. V. Dubonos, I. V. Grigorieva and A. A. Firsov, *Science*, 2004, **306**, 666-669.
4. M. Chhowalla, Z. F. Liu and H. Zhang, *Chem. Soc. Rev.*, 2015, **44**, 2584-2586.
5. V. Nicolosi, M. Chhowalla, M. G. Kanatzidis, M. S. Strano and J. N. Coleman, *Science*, 2013, **340**, 1226419-1226411.
6. J. W. Colson and W. R. Dichtel, *Nat. Chem.*, 2013, **5**, 453-465.
7. R. P. Feynman, *There's Plenty of Room at the Bottom,* 1959. http://www.phy.pku.edu.cn/~qhcao/resources/class/QM/Feynman's-Talk.pdf (access Dec. 2015).
8. T. Bauer, Z. K. Zheng, A. Renn, R. Enning, A. Stemmer, J. Sakamoto and A. D. Schluter, *Angew. Chem. Int. Ed.*, 2011, **50**, 7879-7884.
9. Z. Zheng, C. S. Ruiz-Vargas, T. Bauer, A. Rossi, P. Payamyar, A. Schutz, A. Stemmer, J. Sakamoto and A. D. Schluter, *Macromol. Rap. Commun.*, 2013, **34**, 1670-1680.
10. Z. K. Zheng, L. Opilik, F. Schiffmann, W. Liu, G. Bergamini, P. Ceroni, L. T. Lee, A. Schutz, J. Sakamoto, R. Zenobi, J. VandeVondele and A. D. Schluter, *J. Am. Chem. Soc.*, 2014, **136**, 6103-6110.
11. T. Kambe, R. Sakamoto, K. Hoshiko, K. Takada, M. Miyachi, J. H. Ryu, S. Sasaki, J. Kim, K. Nakazato, M. Takata and H. Nishihara, *J. Am. Chem. Soc.*, 2013, **135**, 2462-2465.

12. R. Dong, M. Pfeffermann, H. Liang, Z. Zheng, X. Zhu, J. Zhang and X. Feng, *Angew. Chem. Int. Ed.*, 2015, **54**, 12058-12063.
13. R. Sakamoto, K. Hoshiko, Q. Liu, T. Yagi, T. Nagayama, S. Kusaka, M. Tsuchiya, Y. Kitagawa, W. Y. Wong and H. Nishihara, *Nat. Commun.*, 2015, **6**.
14. T. Rodenas, I. Luz, G. Prieto, B. Seoane, H. Miro, A. Corma, F. Kapteijn, F. X. L. I. Xamena and J. Gascon, *Nat. Mater.*, 2015, **14**, 48-55.
15. M. Hu, S. Ishihara and Y. Yamauchi, *Angew. Chem. Int. Ed.*, 2013, **52**, 1235-1239.
16. S. C. Junggeburth, L. Diehl, S. Werner, V. Duppel, W. Sigle and B. V. Lotsch, *J. Am. Chem. Soc.*, 2013, **135**, 6157-6164.
17. L. Xu, X. Zhou, Y. Yu, W. Q. Tian, J. Ma and S. Lei, *ACS Nano*, 2013, **7**, 8066-8073.
18. L. Xu, X. Zhou, W. Q. Tian, T. Gao, Y. F. Zhang, S. Lei and Z. F. Liu, *Angew. Chem. Int. Ed.*, 2014, **53**, 9564-9568.
19. J. Y. Yue, X. H. Liu, B. Sun and D. Wang, *Chem. Commun.*, 2015, **51**, 14318-14321.
20. X. H. Liu, C. Z. Guan, S. Y. Ding, W. Wang, H. J. Yan, D. Wang and L. J. Wan, *J. Am. Chem. Soc.*, 2013, **135**, 10470-10474.
21. J. W. Colson, J. A. Mann, C. R. DeBlase and W. R. Dichtel, *J. Pol. Sci. A: Pol. Chem.*, 2015, **53**, 378-384.
22. A. de la Pena Ruigomez, D. Rodriguez-San-Miguel, K. C. Stylianou, M. Cavallini, D. Gentili, F. Liscio, S. Milita, O. M. Roscioni, M. L. Ruiz-Gonzalez, C. Carbonell, D. Maspoch, R. Mas-Balleste, J. L. Segura and F. Zamora, *Chemistry Eur. J.*, 2015, **21**, 10666-10670.
23. P. Payamyar, K. Kaja, C. Ruiz-Vargas, A. Stemmer, D. J. Murray, C. J. Johnson, B. T. King, F. Schiffmann, J. Vandevondele, A. Renn, S. Gotzinger, P. Ceroni, A. Schutz, L. T. Lee, Z. Zheng, J. Sakamoto and A. D. Schluter, *Adv. Mater.*, 2014, **26**, 2052-2058.
24. D. J. Murray, D. D. Patterson, P. Payamyar, R. Bhola, W. Song, M. Lackinger, A. D. Schluter and B. T. King, *J. Am. Chem. Soc.*, 2015, **137**, 3450-3453.
25. J. I. Feldblyum, C. H. McCreery, S. C. Andrews, T. Kurosawa, E. J. Santos, V. Duong, L. Fang, A. L. Ayzner and Z. Bao, *Chem. Commun.*, 2015, **51**, 13894-13897.
26. T.-Y. Zhou, F. Lin, Z.-T. Li and X. Zhao, *Macromol.*, 2013, **46**, 7745-7752.
27. P. Amo-Ochoa, L. Welte, R. Gonzalez-Prieto, P. J. Sanz Miguel, C. J. Gomez-Garcia, E. Mateo-Marti, S. Delgado, J. Gomez-Herrero and F. Zamora, *Chem. Commun.*, 2010, **46**, 3262-3264.
28. Q. Tang, Z. Zhou and Z. Chen, *J. Phys. Chem. C*, 2012, **116**, 4119-4125.
29. P.-Z. Li, Y. Maeda and Q. Xu, *Chem. Commun.*, 2011, **47**, 8436-8438.
30. J. C. Tan, P. J. Saines, E. G. Bithell and A. K. Cheetham, *ACS Nano*, 2012, **6**, 615-621.
31. P. J. Saines, J. C. Tan, H. H. M. Yeung, P. T. Barton and A. K. Cheetham, *Dalton Trans.*, 2012, **41**, 8585-8593.
32. P. J. Saines, M. Steinmann, J. C. Tan, H. H. M. Yeung, W. Li, P. T. Barton and A. K. Cheetham, *Inorg. Chem.*, 2012, **51**, 11198-11209.
33. G. Xu, T. Yamada, K. Otsubo, S. Sakaida and H. Kitagawa, *J. Am. Chem. Soc.*, 2012, **134**, 16524-16527.
34. A. Gallego, C. Hermosa, O. Castillo, I. Berlanga, C. J. Gomez-Garcia, E. Mateo-Marti, J. I. Martinez, F. Flores, C. Gomez-Navarro, J. Gomez-Herrero, S. Delgado and F. Zamora, *Adv. Mater.*, 2013, **25**, 2141-2146.
35. C. Hermosa, B. R. Horrocks, J. I. Martinez, F. Liscio, J. Gomez-Herrero and F. Zamora, *Chem. Sci.*, 2015, **6**, 2553-2558.
36. T. Araki, A. Kondo and K. Maeda, *Chem. Commun.*, 2013, **49**, 552-554.
37. Y. Peng, Y. S. Li, Y. J. Ban, H. Jin, W. M. Jiao, X. L. Liu and W. S. Yang, *Science*, 2014, **346**, 1356-1359.
38. A. Abherve, S. Manas-Valero, M. Clemente-Leon and E. Coronado, *Chem. Sci.*, 2015, **6**, 4665-4673.
39. I. Berlanga, M. L. Ruiz-Gonzalez, J. M. Gonzalez-Calbet, J. L. Fierro, R. Mas-Balleste and F. Zamora, *Small*, 2011, **7**, 1207-1211.
40. I. Berlanga, R. Mas-Balleste and F. Zamora, *Chem. Comm.*, 2012, **48**, 7976-7978.
41. D. N. Bunck and W. R. Dichtel, *J. Am. Chem. Soc.*, 2013, **135**, 14952-14955.
42. S. Chandra, B. P. Biswal, S. Kandambeth, B. Lukose, S. M. Kunjir, M. Chaudhary, R. Babarao, T. Heine and R. Banerjee, *J. Am. Chem. Soc.*, 2013, **135**, 17853-17861.
43. P. Kissel, D. J. Murray, W. J. Wulftange, V. J. Catalano and B. T. King, *Nat. Chem.*, 2014, **6**, 774-778.
44. M. J. Kory, M. Worle, T. Weber, P. Payamyar, S. W. van de Poll, J. Dshemuchadse, N. Trapp and A. D. Schluter, *Nat. Chem.*, 2014, **6**, 779-784.
45. P. Payamyar, K. Kaja, C. Ruiz-Vargas, A. Stemmer, D. J. Murray, C. J. Johnson, B. T. King, F. Schiffmann, J. VandeVondele, A. Renn, S. Gotzinger, P. Ceroni, A. Schutz, L. T. Lee, Z. K. Zheng, J. Sakamoto and A. D. Schluter, *Adv. Mat.*, 2014, **26**, 2052-2058.
46. S.-L. Cai, Y.-B. Zhang, A. B. Pun, B. He, J. Yang, F. M. Toma, I. D. Sharp, O. M. Yaghi, J. Fan, S.-R. Zheng, W.-G. Zhang and Y. Liu, *Chem. Sci.*, 2014, **5**, 4693-4700.
47. D. D. Medina, V. Werner, F. Auras, R. Tautz, M. Dogrut, J. Schuster, S. Linke, M. Döblinger, J. Feldmann, P. Knochel and T. Bein, *ACS Nano*, 2014, **8**, 4042-4052.
48. G. Abellan, C. Marti-Gastaldo, A. Ribera and E. Coronado, *Acc. Chem. Res.*, 2015, **48**, 1601-1611.